

# 超声对激光熔覆 WC 颗粒强化涂层耐磨防腐性能的影响(特邀)

姚喆赫<sup>1,2,3</sup>, 戴温克<sup>1,2,3</sup>, 邹朋津<sup>4</sup>, 余沛炯<sup>4</sup>, 王发博<sup>1,2,3</sup>, 迟一鸣<sup>1,2,3</sup>, 孙振强<sup>1,2,3</sup>, 张群莉<sup>1,2,3</sup>, 姚建华<sup>1,2,3\*</sup>

- (1. 浙江工业大学 激光先进制造研究院, 浙江 杭州 310023;  
2. 特种装备制造与先进加工技术教育部/浙江省重点实验室, 浙江 杭州 310023;  
3. 浙江工业大学 机械工程学院, 浙江 杭州 310023;  
4. 杭州汽轮动力集团股份有限公司, 浙江 杭州 310020)

**摘要:** 面向海洋、矿山等领域机械部件表面耐磨防蚀涂层制备需求, 针对陶瓷颗粒强化涂层高耐磨性能与高耐腐蚀性能难以兼容的问题, 搭建了超声辅助激光熔覆试验平台, 制备了有无超声作用下的碳化钨(WC)颗粒强化涂层。研究了超声对复合涂层微观组织形貌、元素分布、WC 表面合金层厚度的影响规律, 并进一步开展了有无超声试样硬度、摩擦磨损与耐蚀性能测试。结果表明: 超声振动能够细化晶粒, 平均晶粒尺寸从 101.0 μm 降至 59.6 μm, 抑制偏析, 促使 WC 表面合金层溶解与熔覆层元素的均匀分布; 超声作用下, 试样平均显微硬度由 310 HV<sub>0.1</sub> 提升至 425 HV<sub>0.1</sub>, 同时超声作用下 WC 颗粒周围硬度分布更加均匀; 有无超声作用下试样失重量分别为 6.5 mg 和 8.8 mg, 试样磨损率分别为 0.0323 mg/m 和 0.0438 mg/m, 试样磨损率降低了 26.2%; 超声作用下试样腐蚀电流密度由 5.20 μA/cm<sup>2</sup> 降低为 2.13 μA/cm<sup>2</sup>, 同时电化学阻抗谱表明超声作用下试样表面具有更大的电容阻抗环、阻抗模量与相角值。

**关键词:** 激光熔覆; WC 颗粒强化涂层; 超声; 耐磨性能; 防腐性能

**中图分类号:** TN249     **文献标志码:** A     **DOI:** 10.3788/IRLA20230542

## 0 引言

海洋及矿山领域机械装备的叶片、截齿、轴等关键部件长期处于机械磨损与电化学腐蚀的恶劣服役环境<sup>[1]</sup>, 摩擦-腐蚀的交互作用会加速部件表面的破坏损伤, 导致其服役寿命大幅下降<sup>[2]</sup>。为了延长装备的服役寿命、突破基材原有性能的限制, 常采用喷涂<sup>[3]</sup>、电化学沉积<sup>[4]</sup>、原位合成<sup>[5]</sup>、高能束熔融沉积<sup>[6]</sup>等方法在部件表面制备性能优异的强化涂层。其中, 激光熔覆技术因其冶金结合强度好、稀释率低、微观结构精细、力学性能优异等优势, 已被广泛应用于航空、能源、海洋、矿山、冶金等多领域机械部件表面强化涂层的制备<sup>[6]</sup>。

针对部件表面高耐磨损需求, 研究学者采用将碳

化物<sup>[7]</sup>、氮化物<sup>[8]</sup>、氧化物<sup>[9]</sup>等硬质陶瓷颗粒与基体金属粉末进行机械混合, 然后用激光熔覆技术将混合粉末熔覆在基体表面以制备陶瓷颗粒增强金属基复合涂层。其中, 碳化钨(WC)由于其优异的化学稳定性、润湿性与附着力, 已成为激光熔覆强化涂层最常用的陶瓷颗粒之一<sup>[10]</sup>。Benarji 等<sup>[11]</sup>采用激光熔覆技术制备了 SS316-WC 复合强化涂层, 发现 WC 体积分数的增加可以提高涂层的显微硬度与耐磨性能。Li 等<sup>[12]</sup>采用激光熔覆技术制备了不同形状 WC 的 Inconel 625-WC 复合涂层, 发现不同形状的 WC 在激光辐照下分解趋势不同, 球形的 WC 更不易分解产生 W<sub>6</sub>C<sub>2.54</sub>、M<sub>23</sub>C<sub>6</sub> 等硬脆相, 相较于非球形 WC 具有更好的耐磨性能。Wang 等<sup>[13]</sup>采用不同粒径的 WC 颗

收稿日期:2023-09-22; 修訂日期:2023-11-02

基金项目:国家自然科学基金项目(52175443, 52205221); 浙江省“领雁”研发攻关计划项目(2022C01117); 浙江省属高校基本科研业务费专项资金(RF-B2020002)

作者简介:姚喆赫,男,副研究员,博士,主要从事超声复合激光制造方面的研究。

通讯作者:姚建华,男,教授,博士,主要从事激光制造与增材制造的基础与应用方面的研究。

粒制备了激光熔覆强化涂层,发现 WC 颗粒表现出溶解-扩散控制热损伤、坍缩-溶解-扩散控制热损伤和溶解-沉淀控制热损伤的不同特性,进而影响了 WC 颗粒表面合金反应层与枝晶的生长过程、碳化物的析出以及显微组织的均匀性。

研究表明,WC 的引入虽然能提升涂层的耐磨性能,但在高能激光束作用下,WC 颗粒的溶解会改变涂层的物相组成与显微结构<sup>[14]</sup>,进而影响涂层的耐蚀性能。Zhang 等<sup>[15]</sup>制备了不同 WC 含量的 Inconel 625-WC 复合涂层,发现随着 WC 含量的增加,析出碳化物会加剧固溶强化元素的局部偏析,涂层的耐磨性能逐渐提升,但耐腐蚀性能逐渐降低。Li<sup>[16]</sup>研究了 WC 颗粒的含量、形态和分布对激光熔覆涂层组织、力学性能、耐蚀性能和耐磨性能的影响,发现耐蚀性能随着 WC 含量的增加先提高后降低。Jayaraj 等<sup>[17]</sup>研究了 WC 与不同粘结相制备的强化涂层的腐蚀行为,结果表明,WC 与不同粘结相会产生不同显微组织,极大地影响了涂层钝化膜的生成稳定性,进而影响涂层的耐蚀性能。针对激光熔覆强化涂层的组织调控难题,国内外学者在激光熔覆过程中施以电<sup>[18]</sup>、磁<sup>[19]</sup>、热<sup>[20]</sup>、声<sup>[21]</sup>等外加能场辅助控形控性。其中,超声能场在金属熔池中产生的声空化效应、声流效应以及机械效应可以抑制元素偏析、细化晶粒<sup>[22]</sup>、促进增强相均匀分布<sup>[23]</sup>,被认为是能够实现激光熔覆显微组织调控的有效方法。然而,当前超声辅助激光熔覆 WC 颗粒增强涂层的相关研究报道主要集中在耐磨性能的影响,Wang<sup>[24]</sup> 和 Lv<sup>[25]</sup> 采用超声振动辅助激光熔覆制备了 Inconel 718-WC 复合涂层,发现超声振动可降低颗粒的聚集,细化晶粒,提升平均显微硬度和耐磨性能; Nie 等<sup>[26]</sup>研究了超声振幅对激光熔覆 WC 陶瓷颗粒在熔池凝固过程中流动特性的影响,通过改变超声振幅促使 WC 陶瓷颗粒在熔池中逐渐上浮,提升了涂层硬度和耐高温磨损性能。然而,当前超声对 WC 颗粒增强复合涂层的耐蚀性能影响研究较为欠缺,对于耐蚀性能的影响机制尚不明晰,仍需进一步深入研究。

针对激光熔覆 WC 颗粒强化涂层高耐磨性能与高耐腐蚀性能难以兼容的问题,文中将超声振动引入激光熔覆过程,制备了有无超声作用下的 WC 颗粒强

化涂层。分析了超声振动对复合涂层微观组织形貌、元素分布、WC 表面合金层厚度的影响机制,并进一步开展了有无超声试样硬度、摩擦磨损与耐蚀性能测试。相关研究为制备具有高耐磨防腐性能的 WC 颗粒强化涂层提供了参考。

## 1 试验材料与方法

### 1.1 试验材料与设备

试验基体材料为 316L 不锈钢板材,其化学成分如表 1 所示。在开展激光熔覆试验前,打磨板材以去除表面氧化膜,并使用酒精清洗表面污渍后干燥放置备用。试验所用 316L 粉末与 WC 陶瓷颗粒的形貌如图 1(a) 和 (b) 所示,其中 316L 粉末粒径为 70~100 μm,WC 陶瓷颗粒粒径为 50~100 μm,试验前使用行星磨机 (QM-3SP4) 将 316L 粉末与 WC 陶瓷颗粒按质量比 1:4 进行充分混合,将混合粉末置于真空干燥箱进行干燥处理,保温温度 120 ℃,保温时间 60 min。

表 1 316L 不锈钢的化学成分 (wt.%)

Tab.1 Chemical composition of 316L stainless steel

(wt.%)

Composition	Percent	Composition	Percent
C	≤0.03	Si	≤1.0
Cr	16.0-18.0	Mo	2.0-3.0
S	≤0.03	Ni	10.0-14.0
Mn	≤2.0	Fe	Bal.

搭建的超声辅助激光熔覆试验平台如图 1(d) 所示。激光器为半导体激光器 (Laserline, LDF400-2000),最大输出功率为 2 000 W,波长范围 900~1 064 nm,焦距为 25 mm,焦距处的激光光斑为直径 4 mm 的圆形光斑,光斑范围内的能量为平顶分布;运动与控制系统为 6 轴机器人 (ABB, IRB2400-16/1.5),最大速度为 150 (°)/s、轨迹精度与重复定位精度为 0.06 mm;超声振动装置由超声波发生器、换能器、法兰盘、变幅杆以及控制面板等部件组成,其技术指标如表 2 所示,试验前使用螺栓将基体材料固定至超声变幅杆上端面以将超声能量稳定传输至基板;粉末输送与气氛保护气体均为氩气。

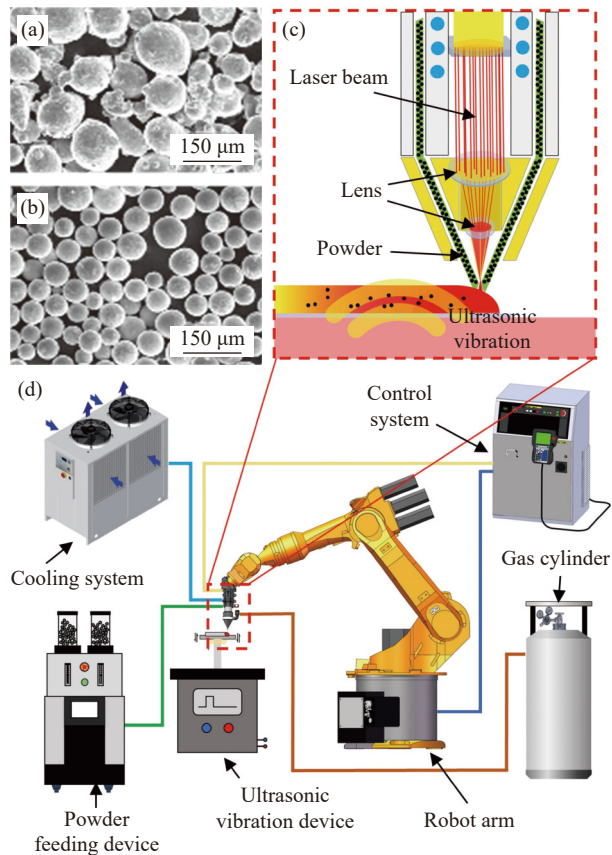


图1 (a) 316L 粉末; (b) WC 粉末; (c) 超声辅助激光熔覆示意图;  
(d) 超声辅助激光熔覆试验平台

Fig.1 (a) 316L powder; (b) WC powder; (c) Schematic diagram of ultrasonic assisted laser cladding; (d) Ultrasonic assisted laser cladding test platform

表2 超声振动装置关键技术指标

Tab.2 Key technical parameters of ultrasonic vibration device

Technical indicator	Parameter	Technical indicator	Parameter
Output power	50-5000 W	Power source	220 V/50 Hz
Frequency	19.5-20.5 kHz	Amplitude	0-50 $\mu\text{m}$
Working radius of the horn	25 mm	Working mode	Gap/Continuity

## 1.2 试验与分析测试方法

试验所用激光功率为 1200 W, 扫描速度为 8 mm/s, 搭接率为 45%, 送粉量为 20 g/min, 保护气流速为 8 L/min, 超声频率为 20 kHz, 超声功率为 2500 W。

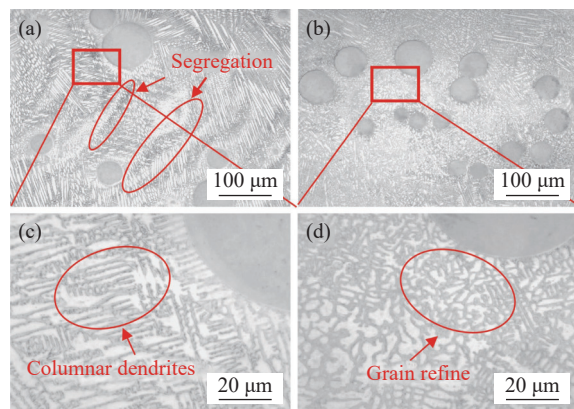
激光熔覆试验后, 采用线切割机对熔覆层进行取样, 尺寸为 7 mm×3 mm×3 mm, 随后进行镶嵌、打磨、抛光、腐蚀。采用光学显微镜 (ZEISS, Axioscope)、扫

描电子显微镜 (ZEISS, EVO18) 以及能谱仪 (EDS, BRUKER XFlash 6130) 对熔覆层的显微组织进行观察分析; 采用自动显微硬度计 (Shimadzu, HMV-2TADWXY) 对熔覆层横截面沿深度方向进行硬度测试, 加载载荷为 100 N, 保荷时间为 10 s, 采用球盘式摩擦磨损仪 (MMQ-02) 进行摩擦磨损测试, 对磨球为  $\text{Si}_3\text{N}_4$  陶瓷球, 直径为 4.75 mm, 测试载荷为 20 N, 磨损轨迹半径 4.0 mm, 电机转速为 200 r/min, 磨损时间为 40 min, 磨损测试前后使用电子秤 (Lichen, FA123C) 对试样称重以获得磨损质量, 采用共聚焦显微镜 (KEYENCE, VK-X1000) 获取试样的三维磨损轮廓以及磨屑的微观形貌, 采用电化学工作站 (CHI760e) 进行耐腐蚀性能测试, 电解质溶液为 3.5% 质量分数的  $\text{NaCl}$  溶液, 工作电极为  $1 \text{ cm}^2$  的铂片电极, 参比电极为饱和甘汞电极, 试样有效面积为  $1 \text{ cm}^2$ 。

## 2 试验结果与讨论

### 2.1 超声对激光熔覆复合涂层微观组织的影响

图2 为有无超声振动作用下激光熔覆复合涂层中 WC 颗粒周围的金相组织, 无超声作用下, WC 周围表现出大量的柱状枝晶以及一部分的元素偏析带, 如图2(a)和(c)所示, 而在超声振动作用下, 试样金相未见明显的偏析带, WC 周围晶粒得到明显细化, 如图2(b)和(d)所示。由于激光熔覆具有快速温升与冷却的特点, 金属熔体凝固时, 晶体易在 WC 外壁上进行非均质形核, 并外延生长形成柱状枝晶, 同时由于部分 WC 溶解导致结晶时元素分布不均匀, 熔覆层易形成偏析带<sup>[27]</sup>, 有无超声作用下的 WC 颗粒强化涂层晶粒分布图如图2(e)如示, 可见相较于无超声作用下



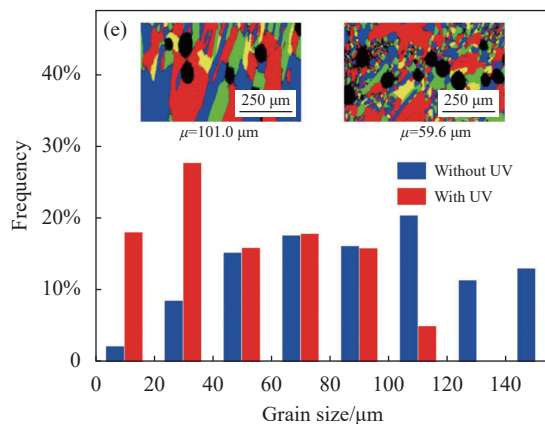


图2 熔覆层WC颗粒周围组织形貌。(a)、(c)无超声;(b)、(d)有超声;(e)晶粒尺寸分布对比

Fig.2 Microstructure morphology around WC particle of cladding layer.  
(a), (c) Without ultrasound; (b), (d) With ultrasound; (e) Comparison of grain size distribution

的晶粒尺寸,有超声作用下WC颗粒周围的晶粒尺寸明显细化,进一步对其晶粒尺寸进行统计,在超声作用下,熔覆层平均晶粒尺寸从101.0 μm降至59.6 μm。

图3为有无超声作用下WC颗粒周围微观组织

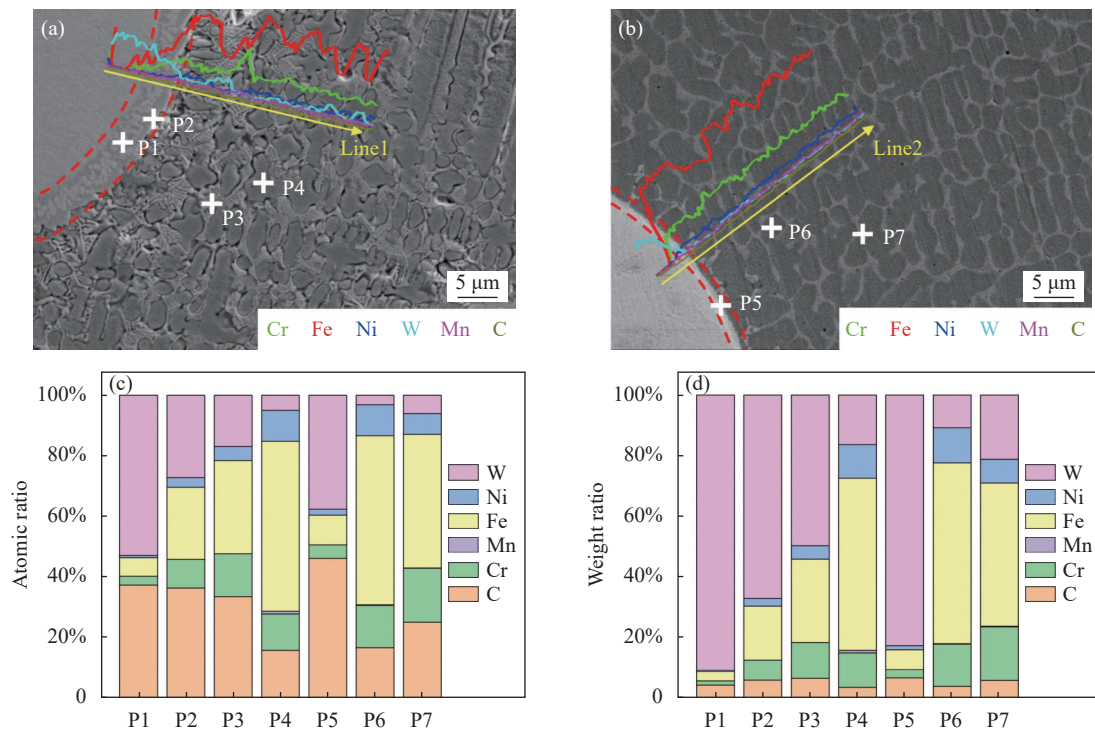


图3 有无超声作用下WC周围微观组织及元素分布。(a)无超声;(b)有超声;(c)原子比对比;(d)质量比对比

Fig.3 Microstructure and element distribution around WC with and without ultrasound action. (a) Without ultrasound; (b) With ultrasound; (c) Comparison of the atomic ratio; (d) Comparison of the mass ratio

的扫描电子显微镜形貌及其元素分布的点扫与面扫结果。无超声作用下,WC表面存在较厚的合金层,此外,在WC颗粒周围分布着大量细小的鱼骨状组织,如图3(a)所示;而在超声作用下,WC表面未见明显的合金层,周围散布着少许网状的析出相,如图3(b)所示。EDS结果表明,在无超声试样中WC表面合金层(P1、P2)中除了含有大量的W元素以外,还富集了Fe、Cr元素,P3为鱼骨状共晶组织,其Fe:(Ni,W)的原子比接近1:1,P4的主要成分为Fe元素;在有超声的试样中,合金反应层明显变薄,点扫描能谱分析(P5)显示Fe、Cr元素富集现象减弱,P6、P7的主要元素均为Fe元素,其中P7的W元素含量稍高于P6。对WC径向进行元素线扫描,从无超声的试样(Line1)强度分布可以看出,在合金反应层中,Fe、W、Cr等元素均沿扩散方向梯度下降,同时在基体中由于存在大量析出相呈现波动变化,而有超声的试样中(Line2),WC与基体间的元素变化梯度更大,这表明合金层很薄,而在基体中各元素的强度变化不大,这是因为超声减少了析出相,均匀了组织。

由于激光的高能量, WC 在熔池中吸收了大量的热量, 分解为游离的 W、C 原子, 当熔池中 W 含量(质量分数)为 35%~52% 时, 即在 WC 颗粒的周围, 熔池中将生成  $W_2C$  和  $Fe_3W_3C$ <sup>[28]</sup>。随着熔池温度不断降低, 在平衡状态下, 熔池中容易生成  $M_6C$ 。故 WC 颗粒在凝固过程中易形成表面合金反应层, P1 由于接近 WC, 含有更高含量的 W 元素, 推测其主要成分为  $W_2C$ ; P2 中 Fe 与 W 元素含量比接近 1:1, 推测其为  $Fe_3W_3C$ , 同时 WC 表面还有 Cr、Ni 等元素参与反应, 整个合金反应层主要成分应为  $W_2C$ 、 $Fe_3W_3C$  和  $M_6C$ (M 为 Fe、W、Cr 和 Ni) 的混合组织, 而周围的组织主要以 316L 的基体相  $\gamma$ -Fe(P4) 为主, 其中夹杂的鱼骨状碳化物(P3)根据其形状与 Fe:(Ni, W) 的原子比推测其为  $Fe_3W_3C$  富铁型碳化物与  $\gamma$ (Fe, Ni) 的共晶组织<sup>[19]</sup>;而在有超声的试样中, 超声的空化作用导致合金层(P5)的溶解变薄, 接近 P1、P2 的中间组成成分; 对比 P4、P6 两点, 发现其元素成分相近, 这是因为超声不会影响熔覆层物相的组织成分, 仅会减少析出相的含量<sup>[24~25]</sup>, P7 是有超声下熔覆层的析出相, 并没有形成微小的鱼骨状碳化物, 这是因为超声的声流作用促进熔池流动, 降低了 WC 颗粒周围的 W 含量, 减少了  $Fe_3W_3C$  的生成, 故超声振动后 WC 颗粒周围组织依然以  $\gamma$ -Fe 为主。

无超声熔覆层中析出的鱼骨状碳化物(P3)其大多属于硬脆相, 极易在 WC 颗粒周围形成梯度的硬度分布, 易产生应力集中, 因而韧性较差, 在摩擦时更易破裂影响耐磨性能。超声对析出相的改善有望提升熔覆层耐磨性能。

为了进一步验证超声对元素分布的影响, 采用面扫描的方式对 WC 周围进行元素分析, 如图 4(a) 所示, 无超声作用时 WC 周围的 W 元素分布在 Fe、Ni 元素之中; 而在施加超声的试样中, 如图 4(b) 所示, Fe、Ni、W 等元素分布相对均匀, 没有明显的夹杂现象。

在激光辐照下, WC 发生分解, 释放出游离的 W 和 C 原子。在随后的快速冷却过程中, 由于时间有限, W 和 C 原子无法迅速扩散到更大的范围, 因此在 WC 颗粒周围形成了富 W 的碳化物, 由于 W 的碳化物具有极高的熔点, 在熔池中更易凝固析出, 会在面扫能谱图中表现出 Fe、Ni 和 W 元素存在交错分布

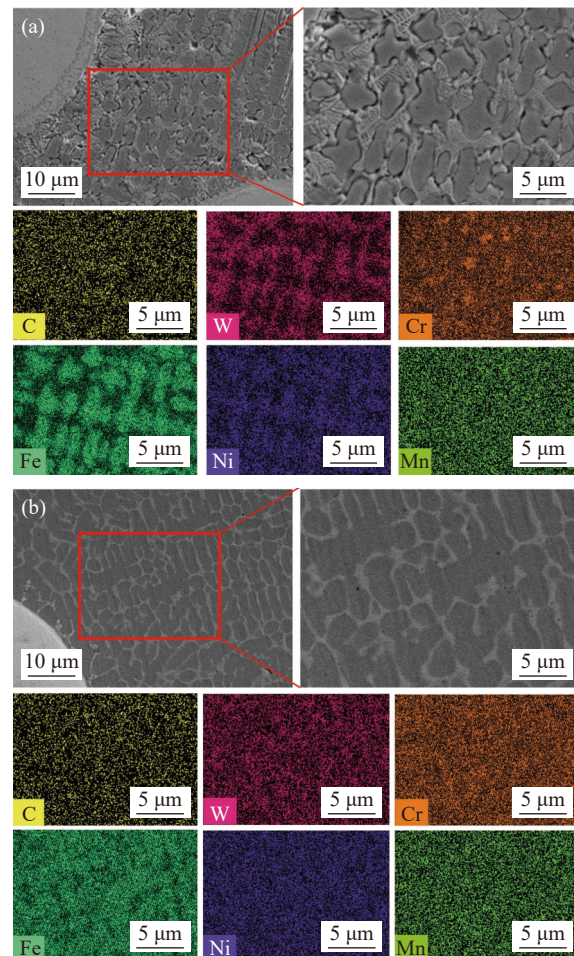


图 4 WC 颗粒周围元素面分布图。(a) 无超声; (b) 有超声  
Fig.4 Surface distribution of elements around WC particle. (a) Without ultrasound; (b) With ultrasound

的现象。而超声的引入, 声流效应加速了熔池流速, 主要的合金元素诸如 Fe、Ni、W 也得以均匀化, 其中 W 元素也因此扩散到更远的距离, 降低了 WC 颗粒周围的 W 元素, 也进一步影响了析出相的生成。

超声的作用机制如图 5 所示, 在激光熔覆过程中, 超声的空化效应会产生大量的空化泡, 空化泡在超声声压与熔体驱使的共同作用下坍缩溃灭。空化气泡的膨胀会吸收周围液体的大量热量, 导致熔池局部区域的过冷; 而空化泡溃灭的瞬间会产生微射流, 破碎在 WC 颗粒表面生长的初生枝晶形成细小均匀的组织结构, 并将其分散到熔池的各个部位, 形成新的形核质点, 这两个因素都有助于提高熔池成核速率<sup>[29]</sup>, 进而导致微观结构的细化。同时, 空化泡溃灭产生局部高温高压促使 WC 表面合金层的溶解, 伴随着超声的声流作用, 这些溶解的合金元素均匀地分布

在整个熔覆层中,可以避免熔池凝固时元素的不均匀分布,抑制偏析。晶粒细化,晶界增加,对位错运动的阻碍增加,材料形变的阻力变大,有利于熔覆层硬度提升。而元素的不均匀会在晶界和晶内形成微原电池反应,加速涂层表面腐蚀,极大地降低熔覆层的耐蚀性能<sup>[30]</sup>,超声可以实现组织和元素的均匀化,有利于减少复合涂层内部的电势差距,减小腐蚀电流,提高涂层的耐蚀性能。

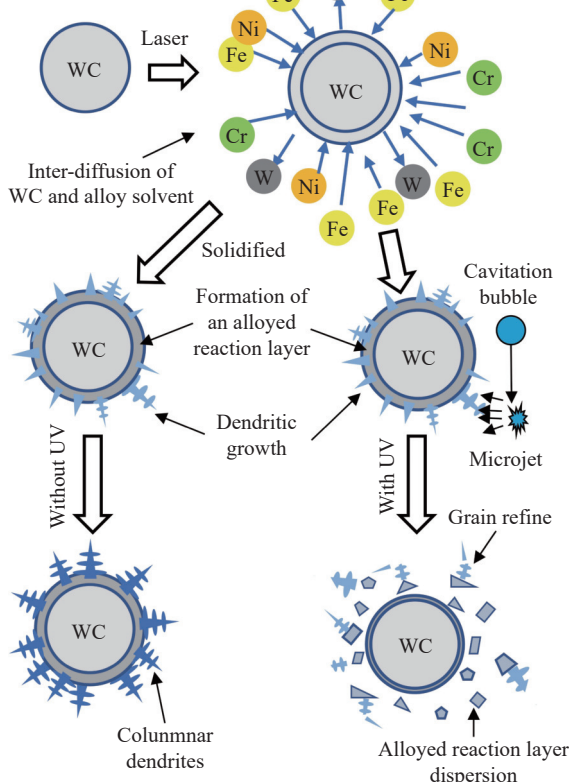


图5 超声对WC合金层与枝晶的作用机制

Fig.5 Mechanism of ultrasonic vibration on WC alloy reaction layer and dendrites

## 2.2 超声对激光熔覆复合涂层硬度分布的影响

图6(a)为有无超声试样横截面沿深度方向的显微硬度分布,测试方向由熔覆层的顶端延伸至基体。相较于基体,无论有无超声作用下的熔覆层显微硬度均有明显提升,熔覆层与基板间热影响区的显微硬度迅速下降,直到达到基体的硬度( $200 \text{ HV}_{0.1}$ )。其中,在无超声试样中,熔覆层硬度分布在 $310 \text{ HV}_{0.1}$ 之间,显微硬度的波动范围为 $75 \text{ HV}_{0.1}$ ,而添加超声的试样熔覆层硬度分布在 $425 \text{ HV}_{0.1}$ 之间,显微硬度的波动范围

为 $30 \text{ HV}_{0.1}$ ,相较于无超声试样显微硬度提升了37%。图6(b)为有无超声作用下WC周围的硬度分布,硬度测试以WC颗粒为中心,间隔 $90^\circ$ ,步距 $40 \mu\text{m}$ 进行打点并计算其平均硬度,无超声作用下,WC四周硬度由 $480 \text{ HV}_{0.1}$ 下降至 $320 \text{ HV}_{0.1}$ ,呈逐步降低的趋势,超声作用下,WC周围硬度分别为 $426 \text{ HV}_{0.1}$ 、 $417 \text{ HV}_{0.1}$ 和 $413 \text{ HV}_{0.1}$ ,分布较为均匀。

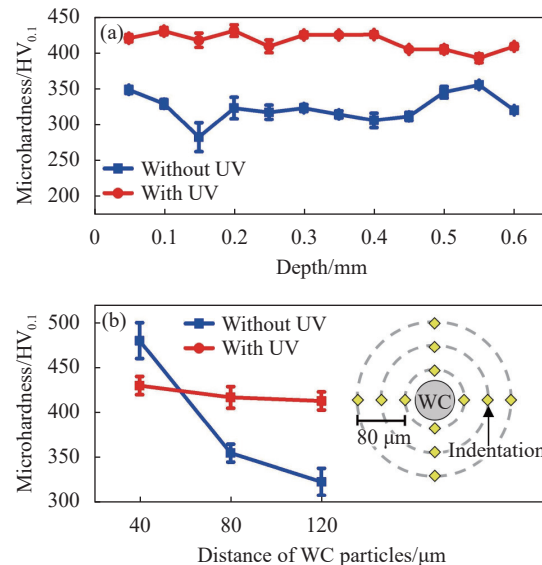


图6 有无超声试样横截面的显微硬度分布。(a) 沿深度方向的硬度分布;(b) WC周围硬度分布

Fig.6 Microhardness distribution of cross sections of samples with and without ultrasound. (a) Hardness distribution along depth; (b) Hardness distribution around WC particle

综合考虑图2~图5,无超声的试样存在大量碳化物析出相,这些碳化物硬度较高,其分布不均匀导致硬度测试出现较大的波动,而超声作用导致WC表面合金层溶解扩散,将W的析出相均匀在整个熔覆层中,不仅提升了硬度性能,还减少了硬度波动的范围。无超声的试样熔覆层中越靠近WC的区域,W、C等对硬度提升较强的元素含量越高,而超声的引入对元素的均匀化减少了元素的梯度变化,表现出更为平缓的硬度梯度分布。综上所述,超声作用在激光熔覆过程中,通过促进WC表面合金层的溶解扩散、均匀元素分布,显著提高了熔覆层的平均硬度并使其分布更加均匀。

## 2.3 超声辅助激光熔覆复合涂层耐磨损性能分析

图7(a)为WC颗粒强化涂层摩擦系数随时间变

化的曲线,在摩擦磨损的初始阶段,摩擦副表面相对光滑,摩擦系数较低。随着摩擦时间的增长,摩擦副接触面积不断扩大,摩擦系数迅速上升。当摩擦副达到相对稳定状态后,无超声的试样摩擦系数围绕 0.6 上下波动,而有超声的试样摩擦系数围绕着 0.5 上下波动。**图 7(b)** 为经过摩擦磨损试验后涂层的质量损失情况,无超声的熔覆层磨损质量为 8.8 mg, 有超声的熔覆层磨损质量为 6.5 mg, 磨损率计算公式如公式(1)所示:

$$M_r = \frac{M}{\pi d N} \quad (1)$$

式中:  $M_r$  为磨损率;  $M$  为质量损失;  $d$  为磨环直径;  $N$  为摩擦磨损旋转转数。

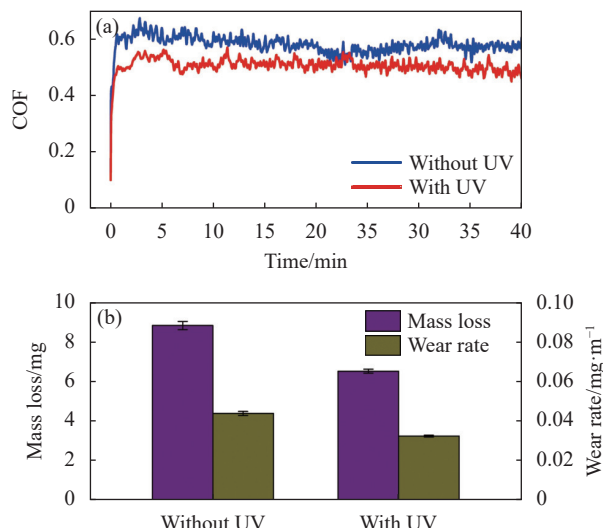


图 7 (a) 有无超声试样摩擦系数曲线;(b) 有无超声下的磨损量与磨损率

Fig.7 (a) Friction coefficient curve of samples with and without ultrasound; (b) Wear amount and wear rate of samples with and without ultrasound

超声的加入使得磨损率从  $0.0438 \text{ mg/m}$  降低到  $0.0323 \text{ mg/m}$ , 降低了 26.2%。同时,无超声作用下涂层摩擦系数呈现先减小再升高的趋势,而超声作用下涂层摩擦系数相对稳定,这是由于无超声作用下涂层组织与硬度分布不均,随着磨痕的深入,由于涂层不同区域硬度存在差异,其耐磨损性能存在差异;而在超声作用下,涂层组织硬度的分布均匀,涂层具有较为一致的耐磨损性能。

**图 8** 为 WC 颗粒强化涂层磨损后磨痕三维形貌,

可以看出均是由磨粒磨损为主,对比**图 8(a)~(d)**可以看出,无超声的试样磨痕犁沟较深,最高深度约为  $53 \mu\text{m}$ ,有超声的试样磨痕犁沟较浅,仅  $26 \mu\text{m}$  左右,但是犁沟底部依然有多处不均匀的起伏,结合磨痕形貌,如**图 8(e)~(f)** 可见,未施加超声的试样有着更深的沟槽,表示其有着更高的磨损率,这与**图 8** 的结果保持一致。

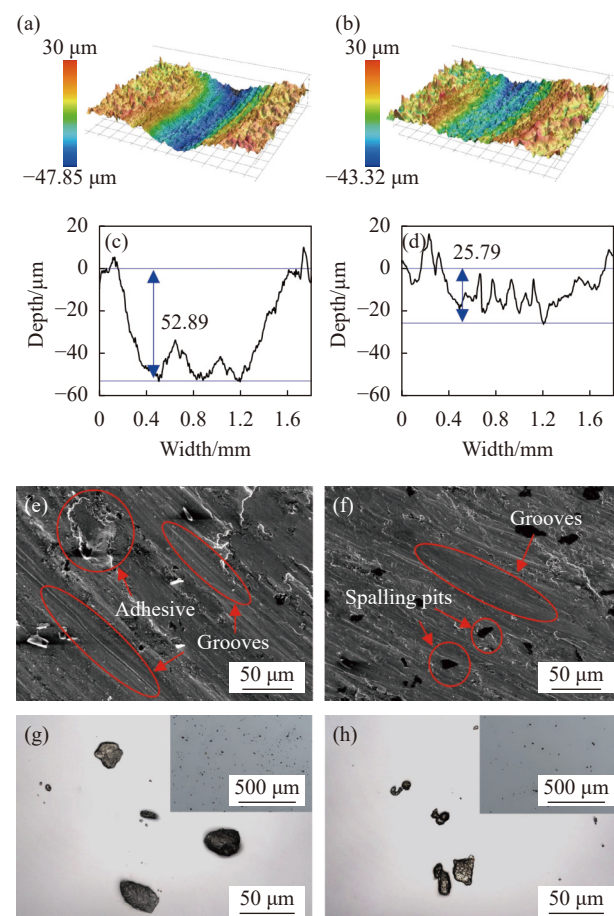


图 8 有无超声试样磨痕轮廓和磨屑貌。(a)、(c)、(e)、(g) 无超声; (b)、(d)、(f)、(h) 有超声

Fig.8 Cross section profile and morphology of the worn surface. (a), (c), (e), (g) Without ultrasound; (b), (d), (f), (h) With ultrasound

此外,相较于未施加超声的试样,磨痕表面有多处细小的剥落坑,进一步采取少量磨屑进行形貌拍摄,可见超声作用下的试样磨屑相较于无超声作用下更为细小。在摩擦磨损时,涂层会剥落一部分磨屑颗粒,对磨损表面产生耕犁和微切削作用,在材料表面留下沟状痕迹,而脱落的磨粒在载荷的作用下会压入摩擦面,并挤压出层片状的磨屑(**图 8(g)**),同时在涂层

中形成犁沟<sup>[31]</sup>;在超声作用下,质地更为坚硬的涂层组织阻碍了磨屑对涂层进一步的磨损,产生了较小的磨屑(图8(h)),犁沟也相对较浅。

#### 2.4 超声辅助激光熔覆复合涂层耐腐蚀性能分析

图9为WC颗粒强化涂层在3.5%氯化钠模拟海水溶液中的动态电位极化曲线,有无超声的试样均表现出相似的曲线走势,分别在-0.40 V和-0.39 V开始发生腐蚀,进入钝化区,随后分别在1.05 V和1.04 V附近钝化膜被击穿发生点蚀,其中无超声的试样腐蚀电流密度曲线高于有超声的试样,在各电位值下都相对较大,腐蚀电流密度分别为5.20  $\mu\text{A}/\text{cm}^2$ 和2.13  $\mu\text{A}/\text{cm}^2$ 。有无超声试样的电化学腐蚀参数如表3所示。

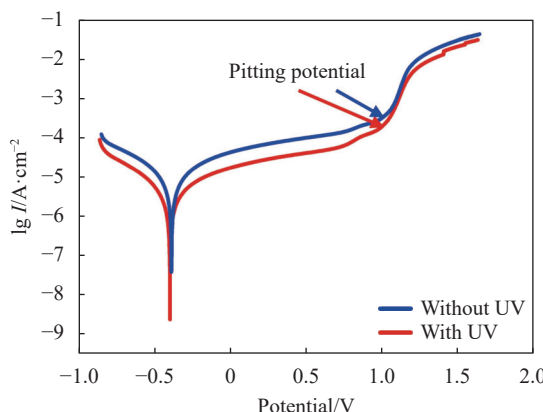


图9 有无超声试样动态电位极化曲线

Fig.9 Dynamic potential polarization curves of samples with and without ultrasound

表3 电化学腐蚀参数

Tab.3 Electrochemical corrosion parameters

	$I_{\text{corr}}/\mu\text{A}\cdot\text{cm}^{-2}$	$E_{\text{corr}}/\text{V}$	$E_{\text{pit}}/\text{V}$
Without UV	5.20	-0.39	1.04
With UV	2.13	-0.40	1.05

为了进一步验证超声对WC颗粒强化涂层耐蚀性能的影响,进行了电化学阻抗谱(EIS)分析,所选择的等效电路模型为 $R(Q(R(QR)))$ ,如图10(c)所示,其中, $R_s$ 表示未补偿溶液电阻, $R_{\text{ct}}$ 表示电荷转移电阻, $R_f$ 表示钝化膜电阻,CPE<sub>1</sub>和CPE<sub>2</sub>表示恒相元件。图10(a)为有无超声作用下的奈奎斯特曲线,其由两个部分组成:实部 $Z'$ 和虚部 $Z''$ 。电容弧表示熔覆层与电解质界面的腐蚀反应,电容阻抗环的半径越大,

其耐腐蚀性越好。超声作用下熔覆层表现出更大的电容弧,即更好的耐蚀性能。图10(b)为有无超声试样的波德图。在低频段,超声作用下试样曲线阻抗模量 $|Z|$ 更高,相角值更大,表明腐蚀界面处存在更致密的钝化膜;在高频范围内,超声作用下的试样曲线同样拥有更高的阻抗模量 $|Z|$ 。一般来说,阻抗模量 $|Z|$ 越大,材料的耐蚀性能越好,相角的振幅与材料的电解质渗透阻力直接相关,较高的相角表示材料渗透阻力增强,具有更好的耐腐蚀性能。对比有无超声作用下

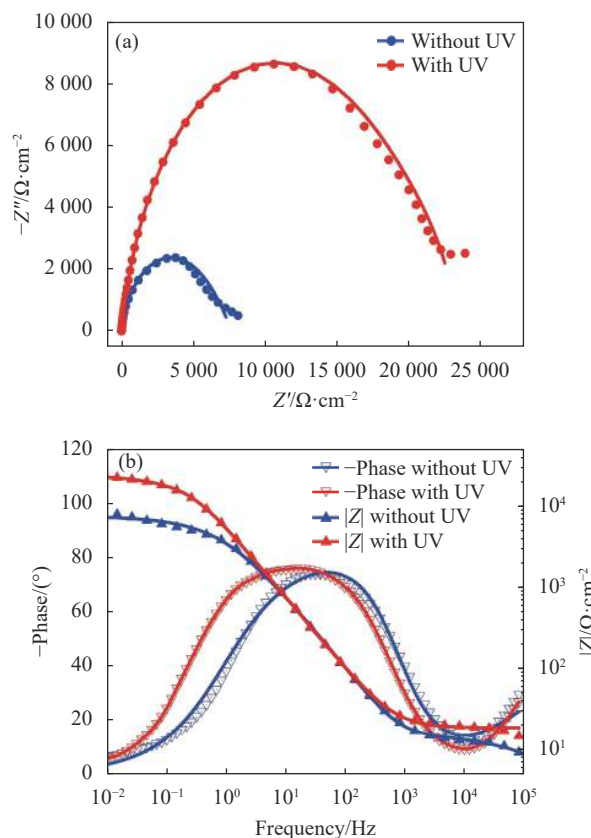


图10 有无超声试样在3.5 wt% NaCl溶液中的阻抗谱。(a)奈奎斯特特图;(b)波德图;(c)等效电路图

Fig.10 EIS of samples in 3.5 wt% NaCl solution with and without ultrasound. (a) Nyquist plot; (b) Bode plot; (d) Equivalent circuit mode

试样的 $|Z|$ 值和相角值,超声作用下的WC颗粒强化涂层具有更强的渗透阻力,即更好的耐腐蚀性能。

由于无超声的试样中组织和元素分布不均匀,这种不均匀的涂层结构会产生微小电流加剧腐蚀,大幅降低材料的耐蚀性能<sup>[32]</sup>。而超声振动的引入不仅会均匀复合涂层中元素的分布,其细化效果还会使得晶粒增加,晶界变多,一般来说,腐蚀通道的增加会降低熔覆层的耐蚀性能,但是超声对熔覆层中元素偏析的抑制提高了元素的均匀程度,减少了局部微原电池的数量,此时更高密度的晶界加速钝化膜的生长,更易形成致密的钝化膜,阻碍阳极反应的进行,整体腐蚀电流降低。同时,均匀的组织和元素分布提高了电解质的渗透阻力,最终提高了其抗腐蚀性能<sup>[33-34]</sup>。

### 3 结 论

文中采用超声辅助激光熔覆技术在316L不锈钢表面制备了WC颗粒强化涂层,对比分析了有无超声作用下涂层的组织形貌、硬度、耐磨性能以及耐腐蚀性能,结果如下:

1) 无超声的熔覆层中,WC周围存在大量柱状晶,同时伴随着部分元素偏析带,由于超声的声空化效应,有超声的熔覆层中WC周围晶粒平均尺寸从101.0 μm降至59.6 μm,没有明显的偏析现象;

2) 无超声 WC 颗粒强化涂层平均显微硬度为 310 HV<sub>0.1</sub>, WC 周围的硬度从 480 HV<sub>0.1</sub>下降到 320 HV<sub>0.1</sub>, 由于超声对组织的均匀化, WC 颗粒强化涂层平均显微硬度为 425 HV<sub>0.1</sub>, WC 周围的硬度从 426 HV<sub>0.1</sub>下降到 413 HV<sub>0.1</sub>;

3) 无超声的试样失重量和磨损率分别为 8.8 mg 和 0.0438 mg/m, 有超声的试样失重量和磨损率分别为 6.5 mg 和 0.0323 mg/m, 无超声的试样磨痕犁沟最大深度约为 53 μm, 有超声的试样磨痕犁沟仅 26 μm 左右, 超声振动对硬度的均匀提升使磨损率显著降低;

4) 有无超声的熔覆层电化学试样腐蚀电流密度分别为 2.13 μA/cm<sup>2</sup> 和 5.20 μA/cm<sup>2</sup>, 超声细化晶粒加速钝化膜生成, 提升了复合涂层的耐蚀性能。

### 参考文献:

- [1] Gou Wenjuan, Zhang Hui, Li Huiping, et al. Effects of silica sand on synergistic erosion caused by cavitation, abrasion, and

- corrosion [J]. *Wear*, 2018, 412-413(C): 120-126.
- [2] Antonyuk M N, Kuptsov K A, Sheveyko A N, et al. Antibacterial TaC-(Fe, Cr, Mo, Ni)-(Ag/Cu) composite coatings with high wear and corrosion resistance in artificial seawater [J]. *Lubricants*, 2022, 10(11): 320.
- [3] Alroy R J, Kamaraj M, Lakshmi D V, et al. Tailoring microstructural features of Cr3C2-25NiCr coatings through diverse spray variants and understanding the high-temperature erosion behavior [J]. *Tribology International*, 2023, 188: 108810.
- [4] Zhao C H, Wang J, Liu T Y, et al. Additive manufacturing of Cu/Ni by selective electrochemical deposition on local conductive substrate [J]. *International Journal of Advanced Manufacturing Technology*, 2023, 126(11-12): 5081-5087.
- [5] Chung S, Lee T, Jeong W, et al. Additive manufacturing of oxide dispersion-strengthened CoCrNi medium-entropy alloy by in situ oxide synthesis [J]. *Journal of Alloys and Compounds*, 2023, 965: 171340.
- [6] Gao D, Wang R, Chen W, et al. Research progress of improving material properties by laser cladding [J]. *Hot Working Technology*, 2017, 46(12): 14-18. (in Chinese)
- [7] Wang W Z, Zhang C, Zhang Z, et al. Effects of carbides on abrasion-corrosion performance of carbide reinforced composites in saline silica slurries [J]. *Wear*, 2023, 526-527: 204949.
- [8] Zhang H W, Cui H Z, Man C, et al. The tribocorrosion resistance of TiN+TiB/TC4 composite coatings and the synergistic strengthening effects of multi-level reinforcements [J]. *Corrosion Science*, 2023, 219: 111224.
- [9] Kumar J K, Rao T B, Krishna K R. The microstructural properties and tribological performance of Al<sub>2</sub>O<sub>3</sub> and tin nanoparticles reinforced Ti-6Al-4V composite coating deposited on AISI304 steel by tig cladding [J]. *Journal of Tribology-Transactions of the Asme*, 2023, 145(1): 011401.
- [10] Li Q, Chen F, Wang Q, et al. Research progress of laser-cladding WC reinforced Ni-based composite coating [J]. *Surface Technology*, 2022, 51(2): 129-143. (in Chinese)
- [11] Benarji K, Kumar Y R, Jinoop A N, et al. Effect of WC composition on the microstructure and surface properties of laser directed energy deposited ss 316-WC composites [J]. *Journal of Materials Engineering and Performance*, 2021, 30(9): 6732-6742.
- [12] Li W L, Di R F, Yuan R W, et al. Microstructure, wear resistance and electrochemical properties of spherical/non-spherical wc reinforced inconel 625 superalloy by laser melting

- deposition [J]. *Journal of Manufacturing Processes*, 2022, 74: 413-422.
- [13] Wang X Y, Zhou S F, Dai X Q, et al. Evaluation and mechanisms on heat damage of WC particles in Ni60/WC composite coatings by laser induction hybrid cladding [J]. *International Journal of Refractory Metals & Hard Materials*, 2017, 64: 234-241.
- [14] Liu H X, Leng N, Zhang X, H, et al. Microstructure and wear behavior of WC/Co50 composite coatings on 40Cr cutting tool surface prepared by laser cladding [J]. *Infrared and Laser Engineering*, 2016, 45(1): 0120001. (in Chinese)
- [15] Zhang K, Ju H C, Xing F, et al. Microstructure and properties of composite coatings by laser cladding inconel 625 and reinforced WC particles on non-magnetic steel [J]. *Optics and Laser Technology*, 2023, 163: 109321.
- [16] Li Ying. Study on the microstructure and erosion wear properties of laser cladding Ni-WC composite coating [D]. Jiaozuo: Henan Polytechnic University, 2021. (in Chinese)
- [17] Jayaraj J, Elo R, Surreddi K B, et al. Electrochemical and passivation behavior of a corrosion-resistant WC-Ni (W) cemented carbide in synthetic mine water [J]. *International Journal of Refractory Metals & Hard Materials*, 2023, 114: 106227.
- [18] Sun Y H, Wang X, Ma Y J, et al. Investigation on improved micro-formability and forming mechanism under high strain rate of H62 brass in pulsed current-assisted laser impact micro-forming [J]. *Materials Science and Engineering: A-Structural Materials Properties Microstructure and Processing*, 2022, 830: 142301.
- [19] Song Shiying, Wang Liang, Hu Yong, et al. Graded coating produced by laser melt injection under steady magnetic field [J]. *Chinese Journal of Lasers*, 2016, 43(5): 0503005. (in Chinese)
- [20] Li L, Mi G Y, Wang C M. A comparison between induction pre-heating and induction post-heating of laser-induction hybrid welding on S690QL steel [J]. *Journal of Manufacturing Processes*, 2019, 43(A): 276-291.
- [21] Yao Zhehe, Shen Qiyan, Ge Hongjiang, et al. Influence of ultrasound on the wetting behavior of molten pool in laser cladding [J]. *Surface Technology*, 2022, 51(10): 20-29. (in Chinese)
- [22] Todaro C J, Easton M A, Qiu D, et al. Grain refinement of stainless steel in ultrasound-assisted additive manufacturing [J]. *Additive Manufacturing*, 2021, 37: 101632.
- [23] Sui C F, Liu Z J, Ai X Y, et al. Effect of ultrasonic vibration on grain size and precipitated phase distribution of 6061 aluminum alloy welded joint [J]. *Crystals*, 2022, 12(2): 240.
- [24] Wang J Z, Zhou J Z, Zhang T, et al. Ultrasonic-induced grain refinement in laser cladding nickel-based superalloy reinforced by WC particles [J]. *Coatings*, 2023, 13(1): 151.
- [25] Lv J, Zhou J Z, Zhang T, et al. Microstructure and wear properties of IN718/WC composite coating fabricated by ultrasonic vibration-assisted laser cladding [J]. *Coatings*, 2022, 12(3): 412.
- [26] Nie Xuewu, Zhou Jianzhong, Xu Jiale, et al. Effect of ultrasound amplitude on microstructure and properties of laser cladding WC/IN718 composite coatings [J]. *Surface Technology*, 2020, 49(9): 206-214. (in Chinese)
- [27] Barr C, Da Sun S, Easton M, et al. Influence of macrosegregation on solidification cracking in laser clad ultra-high strength steels [J]. *Surface & Coatings Technology*, 2018, 340: 126-136.
- [28] Antoni-zdziobek A, Shen J Y, Durand-charre M. About one stable and three metastable eutectic microconstituents in the Fe-W-C system [J]. *International Journal of Refractory Metals & Hard Materials*, 2008, 26(4): 372-382.
- [29] Ramirez A, Qian M, Davis B, et al. Potency of high-intensity ultrasonic treatment for grain refinement of magnesium alloys [J]. *Scripta Materialia*, 2008, 59(1): 19-22.
- [30] Kong D C, Dong C F, Wei S L, et al. About metastable cellular structure in additively manufactured austenitic stainless steels [J]. *Additive Manufacturing*, 2021, 38: 101804.
- [31] Xia Y L, Chen H N, Liang X D, et al. Circular oscillating laser melting deposition of nickel-based superalloy reinforced by WC: Microstructure, wear resistance and electrochemical properties [J]. *Journal of Manufacturing Processes*, 2021, 68: 1694-1704.
- [32] Souza V A D, Neville A. Linking electrochemical corrosion behaviour and corrosion mechanisms of thermal spray cermet coatings (WC-CrNi and WC/CrC-CoCr) [J]. *Materials Science and Engineering a-Structural Materials Properties Microstructure and Processing*, 2003, 352(1-2): 202-211.
- [33] Ralston K D, Birbilis N, Davies C H J. Revealing the relationship between grain size and corrosion rate of metals [J]. *Scripta Materialia*, 2010, 63(12): 1201-1204.
- [34] Xu X, Du J L, Luo K Y, et al. Microstructural features and corrosion behavior of Fe-based coatings prepared by an integrated process of extreme high-speed laser additive manufacturing [J]. *Surface & Coatings Technology*, 2021, 422: 127500.

# Effects of ultrasonic vibration on wear and corrosion resistance of WC particles reinforced coating produced by laser cladding (*invited*)

Yao Zhehe<sup>1,2,3</sup>, Dai Wenke<sup>1,2,3</sup>, Zou Pengjin<sup>4</sup>, Yu Peijiong<sup>4</sup>, Wang Fabo<sup>1,2,3</sup>, Chi Yiming<sup>1,2,3</sup>, Sun Zhenqiang<sup>1,2,3</sup>, Zhang Qunli<sup>1,2,3</sup>, Yao Jianhua<sup>1,2,3\*</sup>

- (1. Institute of Laser Advanced Manufacturing, Zhejiang University of Technology, Hangzhou 310023, China;  
2. Key Laboratory of Special Purpose Equipment and Advanced Processing Technology, Ministry of Education and Zhejiang Province, Hangzhou 310023, China;  
3. College of Mechanical Engineering, Zhejiang University of Technology, Hangzhou 310023, China;  
4. Hangzhou Turbine Power Group Co., Ltd. Hangzhou 310020, China)

## Abstract:

**Objective** Mechanical components in marine and mining fields have long served in harsh environments of mechanical wear and electrochemical corrosion. The interaction of friction and corrosion will accelerate the damage of the component surface and reduce its service life. At present, in order to improve the wear resistance of components, the method of preparing ceramic particle reinforced metal-based composite coating on the surface of the substrate is widely used. Due to the excellent chemical stability, wettability and adhesion, WC particles have become one of the most commonly used ceramic particles in reinforced coating produced by laser cladding. However, under the action of high-energy laser beam, the dissolution of WC particles will change the phase composition and microstructure of the reinforced coating, thus affecting its corrosion resistance. In order to solve the problem that the WC particles reinforced coating is difficult to have both high wear and high corrosion resistance produced by laser cladding, ultrasound is introduced into laser melt injection process. The effects of ultrasonic vibration on the microstructure, microhardness, wear and corrosion resistance of the coating were analyzed. The study provides reference for the preparation of WC particles reinforced coating with high wear and high corrosion resistance.

**Methods** The experimental setup for ultrasonic-assisted laser cladding (Fig.1) is mainly composed of fiber-coupled semiconductor laser, cooling system, motion control system, powder feeder and ultrasonic vibration device. The substrate used in the experiments is 316L stainless steel plate. The powder used in the experiments is a mixed powder of 316 powder and WC particles with the mass ratio of 1 : 4, while the particles size are 70-100  $\mu\text{m}$  and 50-100  $\mu\text{m}$  (Fig.1). Based on the developed experimental setup, the laser cladding experiments with and without ultrasound are carried out. After the experiments, the cross section (perpendicular to the laser scanning direction) and the longitudinal section (parallel to the laser scanning direction) of the laser cladding layer are sampled, polished and etched. The microstructure of the sample was characterized by optical microscope, scanning electron microscope and the chemical composition was determined by EDS analysis. Meanwhile, the hardness, wear and corrosion resistance of the cladding layer were tested.

**Results and Discussions** After ultrasonic assisted laser cladding, the average grain size around WC decreased from 101.0  $\mu\text{m}$  to 59.6  $\mu\text{m}$ , and the surrounding structure and elements are more uniform (Fig.2-4). Due to the effect of ultrasound, the precipitation of fishbone carbide around WC is inhibited. At the same time, the alloy reaction layer on the surface of the WC is dissolved, resulting in the average microhardness of the sample increasing from 310 HV<sub>0.1</sub> to 425 HV<sub>0.1</sub>, and the hardness distribution around the tungsten carbide particles is

more uniform (Fig.6). The wear resistance of the composite coating was further improved by increasing the hardness (Fig.7-8). The mass loss and wear rate of the sample without ultrasonic assisted laser cladding were 8.8 mg and 0.0438 mg/m, respectively, and the maximum depth of the wear mark was about 53 μm. The mass loss and wear rate of the sample with ultrasonic are 6.5 mg and 0.0323 mg/m, respectively, and the maximum depth of the wear marks is about 26 μm. The addition of ultrasound reduced the wear rate by 26.2%. In addition, the introduction of ultrasound did not change the overall corrosion open circuit potential and pitting potential of the cladding layer, but it reduced the corrosion current density (Fig.9), improved the penetration resistance of the corrosive medium on the surface of the coating (Fig.10), and improved the corrosion resistance. Ultrasonic vibration assisted laser cladding can dissolve the alloy reaction layer on the surface of tungsten carbide and increase the hardness of the coating through the uniform distribution of acoustic flow, thus improving the wear resistance of the cladding layer. At the same time, due to the cavitation of ultrasound, the epitaxial growth of columnar dendrites is broken, the grains are refined, and a denser grain boundary is formed. In a corrosive environment, a stable and continuous passivation film can be formed faster because of the increase of the grain boundary, thus improving the corrosion resistance of the WC particles reinforced coating.

**Conclusions** In this paper, ultrasonic assisted laser cladding technology was used to prepare WC particles reinforced coating. The microstructure, hardness, wear and corrosion resistance of the coating under the influence of ultrasound were compared and analyzed. In the non-ultrasonic cladding layer, a large number of columnar crystals existed around WC, accompanied by some element segregation bands, due to the acoustic cavitation effect of ultrasound. The average grain size around WC in the ultrasonic cladding layer is refined from 101.0 μm to 59.6 μm, and there is no obvious segregation phenomenon; The average microhardness of WC particles strengthened coating without ultrasonic is 310 HV<sub>0.1</sub>, and the hardness around WC decreases from 480 HV<sub>0.1</sub> to 320 HV<sub>0.1</sub>. The average microhardness of WC particles strengthened coating with ultrasonic is 425 HV<sub>0.1</sub>, and the hardness around WC decreases from 426 HV<sub>0.1</sub> to 413 HV<sub>0.1</sub>. The weight loss and wear rate of samples without ultrasound were 8.8 mg and 0.0438 mg/m, respectively. The mass loss and wear rate of samples with ultrasound were 6.5 mg and 0.0323 mg/m, respectively. The maximum depth of samples without ultrasonic scratches was about 53 μm, and the maximum depth of samples with ultrasonic was only about 26 μm. The introduction of ultrasound reduced the wear rate by 26.2%. The corrosion current densities of the electrochemical samples with and without ultrasonic are 2.13 μA /cm<sup>2</sup> and 5.20 μA /cm<sup>2</sup>, respectively. Ultrasonic assisted laser cladding of WC particles reinforced coating has better wear and corrosion resistance.

**Key words:** laser cladding; WC particles reinforced coating; ultrasonic vibration; wear resistance; corrosion resistance

**Funding projects:** Natural Science Foundation of China (52175443, 52205221); "Leading Goose" R & D Program of Zhejiang Province (2022C01117); Fundamental Research Funds for the Provincial Universities of Zhejiang (RF-B2020002)